Coplanar-Waveguide Dispersion Characteristics Including Anisotropic Substrates

Chung Jen Hsu, *Member, IEEE*

***Abstract*—An efficient iterative method, based on potential theory, is developed to solve coplanar-waveguide (CPW) dispersion characteristics. In this method, a conformal mapping technique is used to derive the new general expressions for the charge and current sources applicable to both microstrip lines and CPWs. Excellent accuracy for the dispersion results obtained by this method is observed.**

***Index Terms*—Anisotropic substrates, conformal mapping, coplanar waveguide, dispersion, microstrip lines.**

I. Introduction

A COPLANAR waveguide (CPW), consisting of a conductor centered between two ground planes with all on the same plane surface, permits easy shunt connection of external elements in the hybrid and monolithic microwave integrated circuits. Due to the many advantages over microstrip line (MS), CPWs are popularly used as the passive elements in microwave design. Therefore, they naturally attract many researchers to investigate their dispersion characteristics.

Most of the early papers proposing methods to find CPW dispersion characteristics tackled the structure without any enclosure [1]–[3]. Some authors worked out this problem in the spectral domain by formulating the electric-field components in terms of a superposition of TE and TM modes and using very few basis functions for the field components [4], [5]. Although the parasitic effects that occur when coplanar lines are conductor-backed and/or shielded were discussed and evaluated from a quantitative point-of-view in [6], the simple analytical formulas obtained for the dispersive parameters by quasi-static analysis are still questionable for higher frequencies. In [7], a full-wave analysis of CPW dispersions utilizing the time-domain finite-difference method was presented. However, in this approach, the reflections from the artificial walls must be minimized because Fourier transforms are very sensitive to the errors caused by the reflected waves from these boundaries.

In this paper, an efficient iterative novel method based on potential theory is presented to characterize CPW dispersions. As a first step, we utilize conformal mapping to derive the new general expressions for the charge and current on the central strip and ground planes that are valid in the low-frequency limit. To account for high-frequency effects, more terms are included. We then formulate the potential equations from which the propagation constant and characteristic impedance are solved with the help of an iteration technique that is a modified version of the one in [8].

Manuscript received November 2, 1999.

The author was with eWave System Inc., Santa Clara, CA 95054 USA. He is now at 11F No. 25 Dah Rong W. St., Taichung City, Taiwan, R.O.C.

Publisher Item Identifier S 0018-9480(01)01078-X.

II. Derivation of Source Expressions

A CPW to be characterized is shown in Fig. 1(a) and contains two ground planes on each side of the central strip. Obviously, the expressions for the Green's functions have the same forms as those obtained for MSs.

To derive the accurate expressions for the sources, let us consider the geometries shown in Fig. 1(b) and (c) and assume that the coordinates in the $\mathbf{Z}$-plane are transformed to those in the ξ-plane by

$$\mathbf{Z} = \int \frac{\mathbf{D}_0\,\mathrm{d}\xi}{\sqrt{1-\xi^2}} = \mathbf{D}_0 \sin^{-1}\xi + \mathbf{D}_1 \tag{1}$$

where $\mathbf{D}_0 = (2\mathbf{a}/\pi)$ and $\mathbf{D}_1 = 0$. Note that w in the $\mathbf{Z}$-plane is converted to $\sigma_1 = \sin(\pi\mathbf{w}/2\mathbf{a})$ in the ξ-plane, $(w+s)$ is to $\sigma_2 = \sin[\pi(\mathbf{w}+\mathbf{s})/2\mathbf{a}]$, and $\mathbf{a}$ is to 1.

Now take into account the conformal mapping by which Fig. 1(c) is transformed to Fig. 1(d), which is

$$\mathbf{W} = \int \frac{\sigma_2\,\mathrm{d}\xi}{\sqrt{\sigma_1^2-\xi^2}\sqrt{\sigma_2^2-\xi^2}} = \int \frac{\mathrm{d}\lambda}{\sqrt{1-\lambda^2}\sqrt{1-\mathbf{k}^2\lambda^2}} \tag{2}$$

where

$$\lambda = \frac{\xi}{\sigma_1} = \frac{\sin(\pi\mathbf{z}/2\mathbf{a})}{\sin(\pi\mathbf{w}/2\mathbf{a})}$$

and

$$\mathbf{k}^2 = \frac{\sigma_1^2}{\sigma_2^2} = \frac{\sin^2(\pi\mathbf{w}/2\mathbf{a})}{\sin^2[\pi(\mathbf{w}+\mathbf{s})/2\mathbf{a}]}.$$

Note that the point σ_1 in the ξ-plane is transformed to $\mathbf{K}$ in the $\mathbf{W}$-plane and σ_2 to $\mathbf{K}+j\mathbf{K}'$, where $\mathbf{K}$ and $\mathbf{K}'$ are the first- and second-kind complete elliptic integrals, respectively, as calculated by

$$\mathbf{K} = \int_0^1 \frac{\mathrm{d}\lambda}{\sqrt{1-\lambda^2}\sqrt{1-\mathbf{k}^2\lambda^2}} \tag{3a}$$

$$\mathbf{K}' = \int_1^{(1/\mathbf{k})} \frac{\mathrm{d}\lambda}{\sqrt{1-\lambda^2}\sqrt{1-\mathbf{k}^2\lambda^2}}. \tag{3b}$$

Since there is a singular expression existing in the Green's functions when the source and field points coincide, as shown before in earlier papers, such as in [8], it is necessary to extract this first and formulate the dominant part of the integral equations in closed form.

Assume that the Green's function for Fig. 1(b) is $\mathbf{G}_1$ and for Fig. 1(d) is $\mathbf{G}_2$, where one is derived in the original domain and the other is in the transform domain.

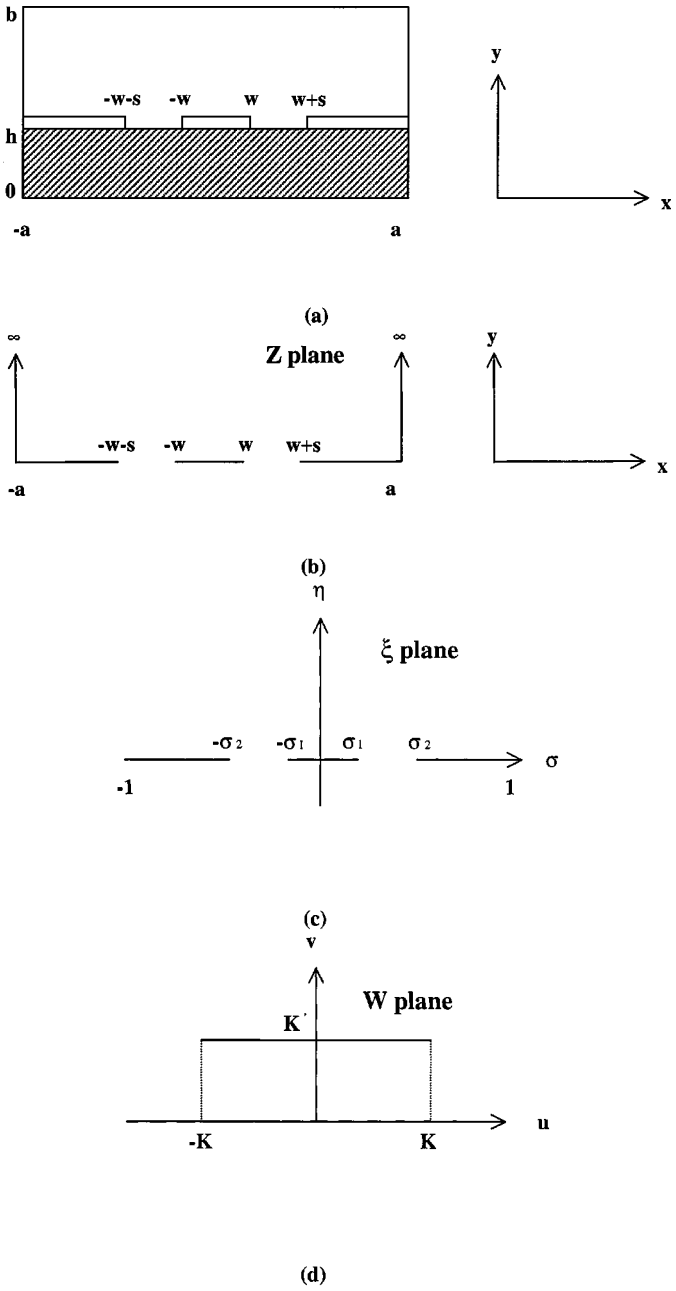

Fig. 1. (a) Shielded CPW (SCPW). (b) Simplified SCPW outline. (c) Transformed configuration of Fig. 1(b) by (1). (d) Transformed configuration of Fig. 1(c) by (2).

From the geometry, the Green's function $\mathbf{G}_1$ satisfies

$$\left(\frac{\partial^2}{\partial \mathbf{x}^2}+\frac{\partial^2}{\partial \mathbf{y}^2}\right)\mathbf{G}_1=-\delta(\mathbf{x}-\mathbf{x}')\,\delta(\mathbf{y}-\mathbf{y}') \tag{4}$$

with these boundary conditions $\mathbf{G}_1 = 0$ at $\mathbf{x} = \pm\mathbf{a}$, $(\partial\mathbf{G}_1/\partial\mathbf{y}) = 0$ at $\mathbf{y} = 0$, and $\mathbf{G}_1 = 0$ at $\mathbf{y} = \infty$.

A reasonable choice of the form for $\mathbf{G}_1$ is

$$\mathbf{G}_1=\sum_{\mathbf{n}=1,\,3}^{\infty}\mathbf{a}_{\mathbf{n}}(\mathbf{y})\cos(\mathbf{u}_{\mathbf{n}}\mathbf{x}) \tag{5a}$$

where $\mathbf{u}_{\mathbf{n}}$ is $\mathbf{n}\pi/2\mathbf{a}$.

Following the same steps as those in [10], we have

$$\left(\frac{\partial^2}{\partial \mathbf{y}^2}+\mathbf{u}_{\mathbf{n}}^2\right)\mathbf{a}_{\mathbf{n}}(\mathbf{y})=-\cos(\mathbf{u}_{\mathbf{n}}\mathbf{x}')\,\delta(\mathbf{y}-\mathbf{y}') \tag{5b}$$

where it is chosen that

$$\mathbf{a}_{\mathbf{n}}(\mathbf{y})=\begin{cases}\mathbf{A}_{\mathbf{n}}\cosh(\mathbf{u}_{\mathbf{n}}\mathbf{y}) & \mathbf{y}\le\mathbf{y}'\\ \mathbf{B}_{\mathbf{n}}\mathbf{e}^{-\mathbf{u}_{\mathbf{n}}(\mathbf{y}-\mathbf{y}')} & \mathbf{y}>\mathbf{y}'.\end{cases}$$

Applying the continuity of $\mathbf{a}_{\mathbf{n}}(\mathbf{y})$ and the discontinuity of its first derivative with respect to y both at $\mathbf{y} = \mathbf{h}$ and solving for the unknowns, we obtain

$$\mathbf{G}_1(\mathbf{x},0;\mathbf{x}',0)=\sum_{\mathbf{n}=1,\,3}^{\infty}\frac{2}{\mathbf{n}\pi}\cos(\mathbf{u}_{\mathbf{n}}\mathbf{x})\cos(\mathbf{u}_{\mathbf{n}}\mathbf{x}') \tag{6}$$

where this $\mathbf{G}_1$ is evaluated at $\mathbf{y} = \mathbf{y}' = 0$.

In the transform domain, we must work out the Green's function for $\mathbf{G}_2$ by solving

$$\left(\frac{\partial^2}{\partial \mathbf{u}^2}+\frac{\partial^2}{\partial \mathbf{v}^2}\right)\mathbf{G}_2=-\delta(\mathbf{u}-\mathbf{u}')\,\delta(\mathbf{v}-\mathbf{v}') \tag{7}$$

with the accompanying boundary conditions $(\partial\mathbf{G}_2/\partial\mathbf{u}) = 0$ at $\mathbf{u} = \pm\mathbf{K}$, $(\partial\mathbf{G}_2/\partial\mathbf{v}) = 0$ at $\mathbf{v} = 0$, and $\mathbf{G}_2 = 0$ at $\mathbf{v} = \mathbf{K}'$.

Using the similar procedures to the above, we obtain, as evaluated at $v = v' = 0$

$$\mathbf{G}_2(\mathbf{u},0;\mathbf{u}',0)=\frac{\mathbf{K}'}{\mathbf{K}}+\sum_{\mathbf{n}=1,\,2}^{\infty}\frac{1}{\mathbf{n}\pi}\cos(\alpha_{\mathbf{n}}\mathbf{u})\cdot\cos(\alpha_{\mathbf{n}}\mathbf{u}')\tanh(\alpha_{\mathbf{n}}\mathbf{K}') \tag{8}$$

where $\alpha_{\mathbf{n}} = \mathbf{n}\pi/\mathbf{K}$.

Although one may note that we select different boundary conditions for the two Green's functions, our inference is founded on the following identity when there are no volume sources:

$$\phi=\oiint\left[\phi\frac{\partial\overline{\mathbf{G}}}{\partial\mathbf{n}}-\overline{\mathbf{G}}\frac{\partial\phi}{\partial\mathbf{n}}\right]\mathbf{dS}_0 \tag{9}$$

which, in this problem, makes us have

$$\begin{aligned}\phi&=\frac{1}{\varepsilon_0}\left[\oiint\mathbf{G}_1\rho_{\mathbf{oc}1}\,\mathbf{dS}_0+\oiint\mathbf{G}_1\rho_{\mathbf{og}1}\,\mathbf{dS}_0\right]\\&=\frac{1}{\varepsilon_0}\oiint\mathbf{G}_2\rho_{\mathbf{oc}2}\,\mathbf{dS}_0\end{aligned} \tag{10}$$

where c denotes the source on the central strip and g stands for the ground planes.

Therefore, it gives the static approximation for the current on the central strip, after we formulate the equation for scalar potential in the transform domain and set it equal to a constant $\mathbf{Q}'$, namely,

$$\int_{-\mathbf{K}}^{\mathbf{K}}\mathbf{G}_2\rho_{\mathbf{oc}}[\mathbf{x}'(\mathbf{u}')]\frac{\mathbf{dx}'}{\mathbf{du}'}\,\mathbf{du}'=\mathbf{Q}'. \tag{11}$$

To ensure that the integration over the range $[-\mathbf{K}, \mathbf{K}]$ is a constant, we choose to set $\rho_{\mathbf{oc}}[\mathbf{x}'(\mathbf{u}')](\mathbf{dx}'/\mathbf{du}') =$ a constant or

$$\rho_{\mathbf{oc}}(\mathbf{x}')=\frac{2}{\mathbf{K}'}\,\mathbf{Q}'\frac{\mathbf{du}'}{\mathbf{dx}'}=\frac{2}{\mathbf{K}'}\,Q'\frac{\mathbf{dW}}{\mathbf{dZ}}.$$

Hence, we have (12), shown at the bottom of the next page.

Note that the current expression is chosen accordingly and that when we set $(w + s)$ equal to a, the structure becomes microstrip and (12) is reduced to the first term in [10, eq. (2.29a)] for microstrip if we further assume that $a \gg w$. Hence, if a is not much larger than w in microstrip, it is suggested that the reduced form of (12) with Chebyshev polynomials in the numer-

ator instead of [10, eq. (2.29)] must be used to achieve greater accuracy.

Since we must include more terms to account for high-frequency effects, we attach some complete functions, like Chebyshev polynomials in microstrip, to the form of (12). Here, we choose the Fourier series in the transform domain as follows:

$$\tilde{\rho}_{\mathbf{oc}}(\mathbf{u}') = \rho_{\mathbf{oc}}\left[\mathbf{x}'(\mathbf{u}')\right]\frac{\mathbf{dx}'}{\mathbf{du}'} = \rho_{\mathbf{oc}}(\mathbf{u}')\frac{\mathbf{dx}'}{\mathbf{du}'} = \sum_{\mathbf{i}=0}^{3}\mathbf{Q_{ci}}\cos(\alpha_{\mathbf{i}}\mathbf{u}') \tag{13}$$

where the subscript denotes the central strip and $\alpha_{\mathbf{i}} = (\mathbf{i}\pi/\mathbf{K})$.

These general expressions are applicable to both a CPW and MS. Therefore, we also use them to obtain the dispersion characteristics for a microstrip, which will be shown later. Besides, the expressions for the sources on the ground planes have the same form as those on the central strip in the transform domain, except that the subscript c is replaced by g.

III. Calculation of the Integrals for Potentials

Since the ground planes must always be taken into account for a CPW, the transverse current is included and expressed in terms of the longitudinal current and the charge by the continuity equations. With these source expressions, we can formulate the potential equations in both the original domain and the transform domain as follows:

$$\begin{aligned}\mathbf{A_{ozr}} = \mu_0 \Bigg[& \int_{-\infty}^{\infty}\int_{-\mathbf{w}}^{\mathbf{w}} \mathbf{G_z}(\mathbf{x},\mathbf{z};\mathbf{x}',\mathbf{z}')\mathbf{J_{ozcr}}(\mathbf{x}') \cdot \mathbf{e^{-j\beta z'}}\,\mathbf{dx'}\,\mathbf{dz'} \\ & + \int_{-\infty}^{\infty}\int_{\mathbf{w+s}}^{\mathbf{a}} \mathbf{G_z}(\mathbf{x},\mathbf{z};\mathbf{x}',\mathbf{z}')\mathbf{J_{ozgr}}(\mathbf{x}') \cdot \mathbf{e^{-j\beta z'}}\,\mathbf{dx'}\,\mathbf{dz'} \\ & + \int_{-\infty}^{\infty}\int_{-\mathbf{a}}^{-(\mathbf{w+s})} \mathbf{G_z}(\mathbf{x},\mathbf{z};\mathbf{x}',\mathbf{z}')\mathbf{J_{ozgr}}(\mathbf{x}') \cdot \mathbf{e^{-j\beta z'}}\,\mathbf{dx'}\,\mathbf{dz'}\Bigg] \\ = \mu_0 \Bigg[& \int_{-\infty}^{\infty}\int_{-\mathbf{K}}^{\mathbf{K}} \mathbf{G_z}(\mathbf{x},\mathbf{z};\mathbf{x}'_{\mathbf{c}},\mathbf{z}')\tilde{\mathbf{J}}_{\mathbf{ozcr}}(\mathbf{u}') \cdot \mathbf{e^{-j\beta z'}}\,\mathbf{du'}\,\mathbf{dz'} \\ & - \int_{-\infty}^{\infty}\int_{\mathbf{K_a}}^{\mathbf{K}} \mathbf{G_z}(\mathbf{x},\mathbf{z};\mathbf{x}'_{\mathbf{g}},\mathbf{z}')\tilde{\mathbf{J}}_{\mathbf{ozgr}}(\mathbf{u}') \cdot \mathbf{e^{-j\beta z'}}\,\mathbf{du'}\,\mathbf{dz'} \\ & - \int_{-\infty}^{\infty}\int_{-\mathbf{K}}^{-\mathbf{K_a}} \mathbf{G_z}(\mathbf{x},\mathbf{z};\mathbf{x}'_{\mathbf{g}},\mathbf{z}')\tilde{\mathbf{J}}_{\mathbf{ozgr}}(\mathbf{u}') \cdot \mathbf{e^{-j\beta z'}}\,\mathbf{du'}\,\mathbf{dz'}\Bigg]\end{aligned} \tag{14a}$$

$$\begin{aligned}\mathbf{A_{ozr}} = \mu_0 \Bigg[& \int_{-\infty}^{\infty}\int_{-\mathbf{w}}^{\mathbf{w}} \mathbf{G_x}(\mathbf{x},\mathbf{z};\mathbf{x}',\mathbf{z}')\mathbf{J_{oxcr}}(\mathbf{x}') \cdot \mathbf{e^{-j\beta z'}}\,\mathbf{dx'}\,\mathbf{dz'} \\ & + \int_{-\infty}^{\infty}\int_{\mathbf{w+s}}^{\mathbf{a}} \mathbf{G_x}(\mathbf{x},\mathbf{z};\mathbf{x}',\mathbf{z}')\mathbf{J_{oxgr}}(\mathbf{x}') \cdot \mathbf{e^{-j\beta z'}}\,\mathbf{dx'}\,\mathbf{dz'} \\ & + \int_{-\infty}^{\infty}\int_{-\mathbf{a}}^{-(\mathbf{w+s})} \mathbf{G_x}(\mathbf{x},\mathbf{z};\mathbf{x}',\mathbf{z}')\mathbf{J_{oxgr}}(\mathbf{x}') \cdot \mathbf{e^{-j\beta z'}}\,\mathbf{dx'}\,\mathbf{dz'}\Bigg] \\ = \mu_0 \Bigg[& \int_{-\infty}^{\infty}\int_{-\mathbf{K}}^{\mathbf{K}} \mathbf{G_x}(\mathbf{x},\mathbf{z};\mathbf{x}'_{\mathbf{c}},\mathbf{z}')\tilde{\mathbf{J}}_{\mathbf{oxcr}}(\mathbf{u}') \cdot \mathbf{e^{-j\beta z'}}\,\mathbf{du'}\,\mathbf{dz'} \\ & - \int_{-\infty}^{\infty}\int_{\mathbf{K_a}}^{\mathbf{K}} \mathbf{G_x}(\mathbf{x},\mathbf{z};\mathbf{x}'_{\mathbf{g}},\mathbf{z}')\tilde{\mathbf{J}}_{\mathbf{oxgr}}(\mathbf{u}') \cdot \mathbf{e^{-j\beta z'}}\,\mathbf{du'}\,\mathbf{dz'} \\ & - \int_{-\infty}^{\infty}\int_{-\mathbf{K}}^{-\mathbf{K_a}} \mathbf{G_x}(\mathbf{x},\mathbf{z};\mathbf{x}'_{\mathbf{g}},\mathbf{z}')\tilde{\mathbf{J}}_{\mathbf{oxgr}}(\mathbf{u}') \cdot \mathbf{e^{-j\beta z'}}\,\mathbf{du'}\,\mathbf{dz'}\Bigg]\end{aligned} \tag{14b}$$

$$\begin{aligned}\phi_o = \frac{1}{\varepsilon_0}\Bigg[& \int_{-\infty}^{\infty}\int_{-\mathbf{w}}^{\mathbf{w}} \mathbf{G}(\mathbf{x},\mathbf{z};\mathbf{x}',\mathbf{z}')\rho_{\mathbf{oc}}(\mathbf{x}') \cdot \mathbf{e^{-j\beta z'}}\,\mathbf{dx'}\,\mathbf{dz'} \\ & + \int_{-\infty}^{\infty}\int_{\mathbf{w+s}}^{\mathbf{a}} \mathbf{G}(\mathbf{x},\mathbf{z};\mathbf{x}',\mathbf{z}')\rho_{\mathbf{og}}(\mathbf{x}') \cdot \mathbf{e^{-j\beta z'}}\,\mathbf{dx'}\,\mathbf{dz'} \\ & + \int_{-\infty}^{\infty}\int_{-\mathbf{a}}^{-(\mathbf{w+s})} \mathbf{G}(\mathbf{x},\mathbf{z};\mathbf{x}',\mathbf{z}')\rho_{\mathbf{og}}(\mathbf{x}') \cdot \mathbf{e^{-j\beta z'}}\,\mathbf{dx'}\,\mathbf{dz'}\Bigg] \\ = \frac{1}{\varepsilon_0}\Bigg[& \int_{-\infty}^{\infty}\int_{-\mathbf{K}}^{\mathbf{K}} \mathbf{G}(\mathbf{x},\mathbf{z};\mathbf{x}'_{\mathbf{c}},\mathbf{z}')\tilde{\rho}_{\mathbf{oc}}(\mathbf{u}') \cdot \mathbf{e^{-j\beta z'}}\,\mathbf{du'}\,\mathbf{dz'} \\ & - \int_{-\infty}^{\infty}\int_{\mathbf{K_a}}^{\mathbf{K}} \mathbf{G}(\mathbf{x},\mathbf{z};\mathbf{x}'_{\mathbf{g}},\mathbf{z}')\tilde{\rho}_{\mathbf{og}}(\mathbf{u}') \cdot \mathbf{e^{-j\beta z'}}\,\mathbf{du'}\,\mathbf{dz'} \\ & - \int_{-\infty}^{\infty}\int_{-\mathbf{K}}^{-\mathbf{K_a}} \mathbf{G}(\mathbf{x},\mathbf{z};\mathbf{x}'_{\mathbf{g}},\mathbf{z}')\tilde{\rho}_{\mathbf{og}}(\mathbf{u}') \cdot \mathbf{e^{-j\beta z'}}\,\mathbf{du'}\,\mathbf{dz'}\Bigg].\end{aligned} \tag{14c}$$

$$\rho_{\mathbf{oc}}(\mathbf{x}') = \frac{\mathbf{Q}'\pi}{\mathbf{K}'\mathbf{a}} \frac{\sin\left[\dfrac{\pi(\mathbf{w}+\mathbf{s})}{2\mathbf{a}}\right]\sqrt{1-\sin^2\left(\dfrac{\pi\mathbf{x}'}{2\mathbf{a}}\right)}}{\sqrt{\sin^2\left[\dfrac{\pi(\mathbf{w}+\mathbf{s})}{2\mathbf{a}}\right]-\sin^2\left(\dfrac{\pi\mathbf{x}'}{2\mathbf{a}}\right)}\sqrt{\sin^2\left(\dfrac{\pi\mathbf{w}}{2\mathbf{a}}\right)-\sin^2\left(\dfrac{\pi\mathbf{x}'}{2\mathbf{a}}\right)}} \tag{12}$$

In the above integrals, $\mathbf{G}$ and $\mathbf{G_z}$ are the Green's functions shown in [9] and [10]. $\mathbf{K_a}$ and the evaluations of $\mathbf{x_c'}$ and $\mathbf{x_g'}$ in terms of u' are, respectively, given by

$$\mathbf{K_a} = \mathbf{K} - \int_{1/\mathbf{k}}^{1/\sigma_1} \frac{\mathbf{d}\lambda}{\sqrt{\lambda^2-1}\sqrt{\mathbf{k}^2\lambda^2-1}} \tag{15a}$$

$$\mathbf{x_c'} = \frac{\mathbf{2a}}{\pi}\sin^{-1}\left[\sin\left(\frac{\pi \mathbf{w}}{\mathbf{2a}}\right)\mathbf{sn}(\mathbf{u'}, \mathbf{k})\right] \tag{15b}$$

$$\mathbf{x_g'} = \frac{\mathbf{2a}}{\pi}\sin^{-1}\left[\sin\left(\frac{\pi \mathbf{w}}{\mathbf{2a}}\right)\mathbf{sn}(\mathbf{u'} + \mathbf{jK'}, \mathbf{k})\right] \tag{15c}$$

where $\mathbf{sn}(\mathbf{u'}) = \sin.\mathbf{am}(\mathbf{u'})$ is one of Elliptic functions.

There is a singularity in the Green's function, which accounts for the dominant part, arising when the field and source points coincide. Therefore, we can compute the integrals of the Green's functions first with respect to z' to extract this term as follows:

$$\begin{aligned}\hat{\mathbf{G}}_\mathbf{z}&(\mathbf{x}, \mathbf{z}; \mathbf{x_c'}) \\ &= \int_{-\infty}^{\infty} \mathbf{G_z}(\mathbf{x}, \mathbf{z}; \mathbf{x_c'}, \mathbf{z'})\mathbf{e}^{-\mathbf{j}\beta \mathbf{z'}}\,\mathbf{dz'} \\ &= \left\{\frac{2}{\mathbf{a}}\sum_{\mathbf{n}=1,3}^{\infty}[\mathbf{TF(n)} - \mathbf{AF(n)}]\cos(\mathbf{u_n x})\cos(\mathbf{u_n x_c'}) \right. \\ &\quad \left. + \frac{1}{\pi}\sum_{\mathbf{n}=1,3}^{\infty}\frac{1}{\mathbf{n}}\cos(\mathbf{u_n x})\cos(\mathbf{u_n x_c'})\right\}\mathbf{e}^{-\mathbf{j}\beta \mathbf{z}}\end{aligned} \tag{16a}$$

$$\begin{aligned}\hat{\mathbf{G}}&(\mathbf{x}, \mathbf{z}; \mathbf{x_c'}) \\ &= \int_{-\infty}^{\infty} \mathbf{G}(\mathbf{x}, \mathbf{z}; \mathbf{x_c'}, \mathbf{z'})\mathbf{e}^{-\mathbf{j}\beta \mathbf{z'}}\,\mathbf{dz'} \\ &= \left\{\frac{2}{\mathbf{a}}\sum_{\mathbf{n}=1,3}^{\infty}[\mathbf{TG(n)} - \mathbf{AG(n)}]\cos(\mathbf{u_n x})\cos(\mathbf{u_n x_c'}) \right. \\ &\quad \left. + \kappa_\mathbf{r}\frac{2}{\pi}\sum_{\mathbf{n}=1,3}^{\infty}\frac{1}{\mathbf{n}}\cos(\mathbf{u_n x})\cos(\mathbf{u_n x_c'})\right\}\mathbf{e}^{-\mathbf{j}\beta \mathbf{z}}\end{aligned} \tag{16b}$$

where the parameter x can be $\mathbf{x_c}$ or $\mathbf{x_g}$ and $TF(n)$, $AF(n)$, $TG(n)$, $AG(n)$, and $\kappa_\mathbf{r}$ are defined in [10, App.].

At present, calculating the remaining integration of the integrals in the transform domain over u' after substituting (13) into (14) shows that we have these results for the correction terms

$$\mathbf{t_{ni}} = 2\int_0^{\mathbf{K}} \cos(\mathbf{u_n x_c'})\cos(\alpha_\mathbf{i} \mathbf{u'})\,\mathbf{du'} \tag{17a}$$

$$\mathbf{s_{ni}} = 2\int_{\mathbf{K_a}}^{\mathbf{K}} \cos(\mathbf{u_n x_g'})\cos(\alpha_\mathbf{i} \mathbf{u'})\,\mathbf{du'}. \tag{17b}$$

Note that these expressions are also the testing results when we apply the testing functions $\sum_{\mathbf{i}=0}^{3}\cos(\alpha_\mathbf{i}\mathbf{u})$ to the central strip and ground planes.

For the dominant terms, the summation over n is manipulated into the same form as in [10, eq. (2.36)]. After testing, we then have over u

$$\begin{aligned}\mathbf{t_{ji}} = -\int_0^{\mathbf{K}}\int_0^{\mathbf{K}} &\ln\left|\tan\left[\frac{\pi(\mathbf{x_c} - \mathbf{x_c'})}{4\mathbf{a}}\right]\right. \\ &\left.\cdot\tan\left[\frac{\pi(\mathbf{x_c} + \mathbf{x_c'})}{4\mathbf{a}}\right]\right|\cos(\alpha_\mathbf{i}\mathbf{u'})\cos(\alpha_\mathbf{j}\mathbf{u})\,\mathbf{du'}\,\mathbf{du}\end{aligned} \tag{18a}$$

$$\begin{aligned}\mathbf{s_{ji}} = -\int_{\mathbf{K_a}}^{\mathbf{K}}\int_{\mathbf{K_a}}^{\mathbf{K}} &\ln\left|\tan\left[\frac{\pi(\mathbf{x_g} - \mathbf{x_g'})}{4\mathbf{a}}\right]\right. \\ &\left.\cdot\tan\left[\frac{\pi(\mathbf{x_g} + \mathbf{x_g'})}{4\mathbf{a}}\right]\right|\cos(\alpha_\mathbf{i}\mathbf{u'})\cos(\alpha_\mathbf{j}\mathbf{u})\,\mathbf{du'}\,\mathbf{du}\end{aligned} \tag{18b}$$

$$\begin{aligned}\mathbf{c_{ji}} = -\int_0^{\mathbf{K}}\int_{\mathbf{K_a}}^{\mathbf{K}} &\ln\left|\tan\left[\frac{\pi(\mathbf{x_c} - \mathbf{x_g'})}{4\mathbf{a}}\right]\right. \\ &\left.\cdot\tan\left[\frac{\pi(\mathbf{x_c} + \mathbf{x_g'})}{4\mathbf{a}}\right]\right|\cos(\alpha_\mathbf{i}\mathbf{u'})\cos(\alpha_\mathbf{j}\mathbf{u})\,\mathbf{du'}\,\mathbf{du}\end{aligned} \tag{18c}$$

$$\begin{aligned}\mathbf{d_{ji}} = -\int_{\mathbf{K_a}}^{\mathbf{K}}\int_0^{\mathbf{K}} &\ln\left|\tan\left[\frac{\pi(\mathbf{x_g} - \mathbf{x_c'})}{4\mathbf{a}}\right]\right. \\ &\left.\cdot\tan\left[\frac{\pi(\mathbf{x_g} + \mathbf{x_c'})}{4\mathbf{a}}\right]\right|\cos(\alpha_\mathbf{i}\mathbf{u'})\cos(\alpha_\mathbf{j}\mathbf{u})\,\mathbf{du'}\,\mathbf{du}\end{aligned} \tag{18d}$$

where $\mathbf{t_{ji}} = \mathbf{t_{ij}}$ and $\mathbf{s_{ji}} = \mathbf{s_{ij}}$ are the self-testing results and $\mathbf{c_{ji}} = \mathbf{d_{ij}}$ are the cross-testing results.

For the self-testing results, only part of the terms need calculating numerically, while all terms for either of the cross-testing results must be computed. Since there are singularities in each logarithm function for self-testing, special treatment is taken when we perform the integration by a numerical method.

IV. Modified Iteration Technique

In MSs, there is no dominant-mode transverse current $\mathbf{J_{oxr}}$ assumed on the strip since its effect is negligible for a wide range of useful geometries. However, this is not true for CPWs, especially when the ground planes must always be taken into consideration.

Therefore, unlike MSs where the assumptions $\mathbf{A_{ozr}}/\mu_0 = 1$ and $\varepsilon_0\phi_\mathbf{o} = 1$ are made to execute the iteration method, we have to use the boundary conditions that the tangential components of the electric fields must vanish on both the central strip and ground planes.

By utilizing $\mathbf{E_z} = -\mathbf{j}(\beta \mathbf{c}/\mathbf{k}_0)\mathbf{A_{ozr}} - \partial\phi/\partial\mathbf{z} = 0$ and $\mathbf{E_x} = -\mathbf{j}(\beta \mathbf{c}/\mathbf{k}_0)\mathbf{A_{oxr}} - \partial\phi/\partial\mathbf{x} = 0$ and applying the moment method, we can generate a set of linear equations. Note that, in evaluating $\mathbf{A_{oxr}}$, [10, eqs. (3.18) and (3.19)] are again taken advantage of, and we utilize $\mathbf{J_{xcr}}(\boldsymbol{w}, \mathbf{z}) = 0$ and $\mathbf{J_{xgr}}(\mathbf{w} + \mathbf{s}, \mathbf{z}) = 0$, which are mathematically proven.

Since there is $\sin(\mathbf{u_n x})$ in $\mathbf{E_x}$ instead of $\cos(\mathbf{u_n x})$, we perform the incomplete integration of $\mathbf{E_x}$ over x first to facilitate the use of the existing testing results, namely, (17). Note that

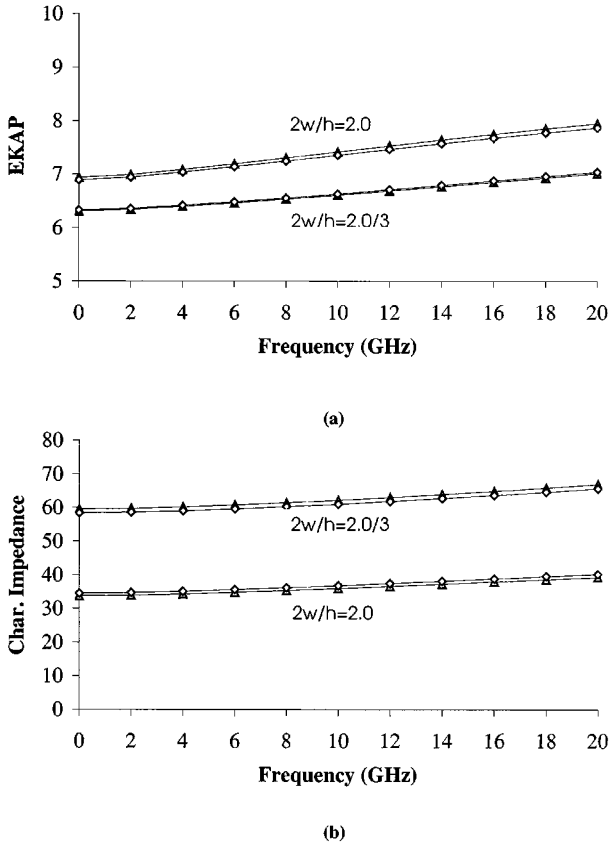

Fig. 2. (a) MS effective dielectric constant for an alumina substrate where $h = 0.635$ mm, $a = 10$ mm, and $c = 10.365$ mm for both cases. —Δ—: the method in [10, Ch. 2], —◇—: this paper. (b) Characteristic impedance for the MS of Fig. 2(a).

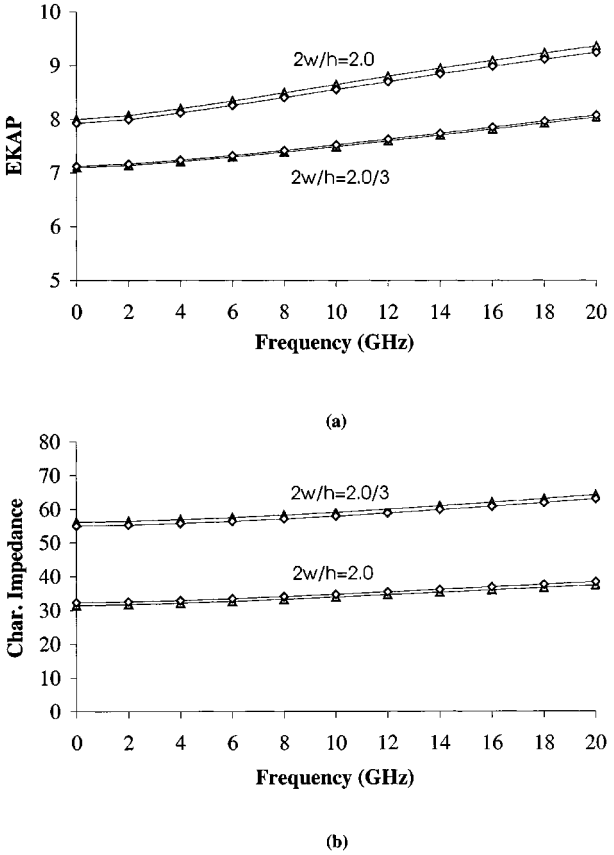

Fig. 3. (a) MS effective dielectric constant for a sapphire substrate where $h = 0.635$ mm, $a = 10$ mm, and $c = 10.365$ mm for both cases. —Δ—: the method in [10, Ch. 2], —◇—: this paper. (b) Characteristic impedance for the MS of Fig. 3(a).

it is also adopted in our software programs for the microstrip gap discontinuity for the computational time-saving purpose and improved accuracy.

Similarly, using a trial value of β, the unknowns for $\mathbf{Q_{c,gi}}$ and $\mathbf{I_{c,gi}}$ are found from this matrix. Now, the total charge and relative current on the central strip are given by $\mathbf{I_{Tc}} = 2\mathbf{K}\mathbf{I_{c0}}$ and $\mathbf{Q_{Tc}} = 2\mathbf{K}\mathbf{Q_{c0}}$.

A new estimate of the propagation constant can be calculated from [10, eq. (2.37)] where $\varepsilon_{\mathbf{em}}$ is replaced by $\varepsilon_{\mathbf{ec}} = \mathbf{Q_{Tc}}/\mathbf{I_{Tc}} = \mathbf{Q_{c0}}/\mathbf{I_{c0}}$ defined as effective dielectric constant for CPW. If the new value of ε_{ec} differs from the old value of ε_{ec} by less than 1%, the iteration is terminated; otherwise, the iteration is repeated with the fact that the latest values of β, $\mathbf{Q_{c,gi}}$, and $\mathbf{I_{c,gi}}$ are used as the new entries in the matrix for each successive iteration until the condition is satisfied. By this way, the iteration converges very fast for CPW dispersion problems.

After a convergent value of ε_{ec} is found, the characteristic impedance of CPW is computed. And, it is defined as the ratio of the voltage between the center of the central strip and the ground planes to the total current flowing along the central strip. Since $\mathbf{A_{ox}}$ can also be expressed in terms of Fourier series form so that we have (19), shown at the bottom of this page, where $\mathbf{I^c_{TOT}}$ is the total z-directed current on the central strip, $\mathbf{J_{zcrn}}$ and ρ_{cn} are defined as

$$\mathbf{J_{zcrn}} = \frac{2}{\mathbf{a}} \sum_{\mathbf{i=0}}^{3} (\mathbf{I_{ci}}\mathbf{t_{ni}} + \mathbf{I_{gi}}\mathbf{s_{ni}}) \tag{20a}$$

$$\rho_{\mathbf{cn}} = \frac{2}{\mathbf{a}} \sum_{\mathbf{i=0}}^{3} (\mathbf{Q_{ci}}\mathbf{t_{ni}} + \mathbf{Q_{gi}}\mathbf{s_{ni}}) \tag{20b}$$

$$\mathbf{Z^c_c} = \frac{1}{\mathbf{I^c_{TOT}}} \int_{(\mathbf{w+s})}^{0} -\mathbf{E_x}\,\mathbf{dx} = \frac{1}{\mathbf{I^c_{TOT}}} \int_{(\mathbf{w+s})}^{0} \left(\frac{\partial \phi}{\partial \mathbf{x}} + \mathbf{j}\omega\mathbf{A_{ox}}\right)_{\mathbf{y=h}} \mathbf{dx} = \frac{60\pi}{\mathbf{K}\sqrt{\mathbf{I_{c0}}\mathbf{Q_{c0}}}}$$
$$\cdot \left[1 + \mathbf{k_0^2} \sum_{\mathbf{n=1,3}}^{\infty} \frac{\rho_{\mathbf{cn}} - \varepsilon_{\mathbf{ec}}\mathbf{J_{zcrn}}}{\mathbf{u_n}} \frac{\sinh(\zeta_{\mathbf{n}}\mathbf{c})\sinh(\zeta_{1\mathbf{n}}\mathbf{h})}{\left[\zeta_{1\mathbf{n}}\sinh(\zeta_{\mathbf{n}}\mathbf{c})\cosh(\zeta_{1\mathbf{n}}\mathbf{h}) + \zeta_{\mathbf{n}}\cosh(\zeta_{\mathbf{n}}\mathbf{c})\sinh(\zeta_{1\mathbf{n}}\mathbf{h})\right]} \frac{\cos\left[\mathbf{u_n}(\mathbf{w+s})\right] - 1}{\mathbf{u_n}}\right] \tag{19}$$

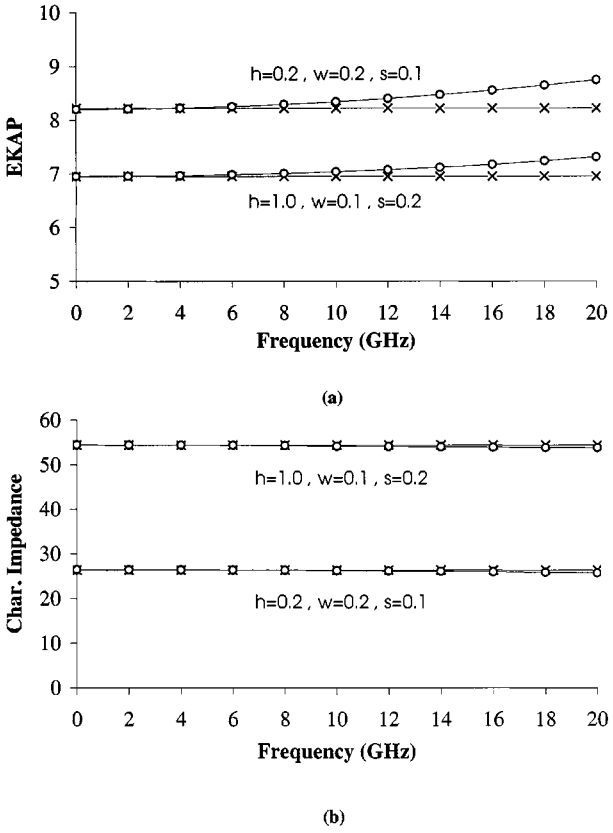

Fig. 4. (a) CPW effective dielectric constant for a GaAs substrate where $a = 1$ mm, $c = 1$ mm, and CPW dimensions all in mm for both cases. —×—: [6], —○—: this paper. (b) Characteristic impedance for the CPW of Fig. 4(a).

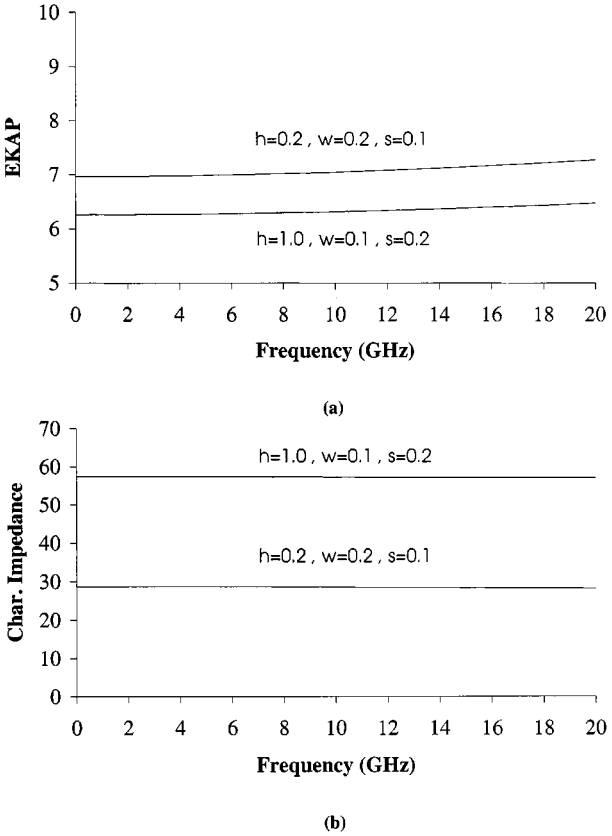

Fig. 5. (a) CPW effective dielectric constant for an Epsilam-10 substrate where $a = 1$ mm, $c = 1$ mm, and CPW dimensions all in millimeters for both cases. (b) Characteristic impedance for the CPW of Fig. 5(a).

which are the coefficients associated with their Fourier series expansions for the sources in the original domain, and all of the other quantities in (19) are the same as before.

V. Results

Many ways are used to verify the validity of our method. First of all, our results obtained in the transformed domain from the general expressions for the sources are checked against those by the method in [10, Ch. 2] for MS dispersions including anisotropic substrates. Since the method in [10, Ch. 2] was developed in the original domain, it produces almost the same results as those in [8], discussed and compared with a lot of the results shown by many other authors.

We compute the MS dispersion data shown in Fig. 2(a) and (b) for an alumina substrate whose typical dielectric constant is quoted as 9.7. Fig. 3(a) and (b) gives the MS dispersion data for a sapphire substrate with $\kappa = 9.4$ and $\kappa_y = 11.6$. All the lines in these four figures with diamond marks are our results by the method in [10, Ch. 2] and the other lines with triangular marks are our results by the method in this paper.

In addition, we examine the results produced by this method for CPW dispersions against those that were given by the quasi-static approximation equation in [6]. This equation was derived by assuming that the semi-infinite ground planes on each side of the central strip, which, as mentioned above, contradicts the real structures usually encountered. Also, we find that the finite widths of the ground planes do influence the dispersions to some extent and this fact was not taken into consideration in the quasi-static equation. Since this structure of a CPW can support a perturbed TE_{10} rectangular waveguide mode, this phenomenon results in a limitation for the width of the dielectric-loaded waveguide; namely, the value of a.

The CPW dispersion data for a GaAs substrate using the dielectric constant $\kappa = 12.9$ are shown in Fig. 4(a) and (b). The lines with circle marks are our results and the other lines with crossmarks are those by the quasi-static equation. We use an Epsilam-10 substrate as an example to obtain the CPW dispersion data, with anisotropic substrates, as shown in Fig. 5(a) and (b). The substrate has anisotropic dielectric constant with $\kappa = 13$ and $\kappa_y = 10.3$. In all four figures, our results with both isotropic and anisotropic substrates show a slight increase for effective dielectric constants with frequency and a very slight decrease for characteristic impedances against frequency. Note that only by halving the dimensions of the CPW, the data discussed in this paper can be used to cover the frequency range from 0 to 40 GHz.

VI. Conclusion

In this paper, we have presented an efficient and accurate novel method, founded on potential theory, to treat CPW dispersion characteristics with the help of an iteration approach. In the method, a conformal mapping technique is used to obtain the new general expressions for the sources that can be also applied to MSs. The data produced by this method shows rela-

tively good accuracy for both CPWs and MSs having isotropic and anisotropic substrates. The CPU time to obtain eleven sets of data is 47 s on a Sun IPC workstation. We are currently extending the novel method to treat finlines including anisotropic substrates.

ACKNOWLEDGMENT

The author would like to thank his doctoral advisor, Dr. R. E. Collin, Case Western Reserve University, Cleveland, OH, for the valuable discussions and help.

REFERENCES

[1] C. P. Wen, "Coplanar waveguide—A surface strip transmission line suitable for nonreciprocal gyromagnetic device applications," *IEEE Trans. Microwave Theory Tech.*, vol. MTT-17, pp. 1087–1091, Dec. 1969.

[2] M. E. Davies, E. W. Williams, and A. C. Celestine, "Finite boundary corrections to the coplanar waveguide analysis," *IEEE Trans. Microwave Theory Tech.*, vol. MTT-21, pp. 594–596, Sept. 1973.

[3] A. Gopinath, "Losses in coplanar waveguide," *IEEE Trans. Microwave Theory Tech.*, vol. MTT-23, pp. 1101–1104, July 1982.

[4] J. B. Knorr and K. D. Kuchler, "Analysis of coupled slots and coplanar strips on dielectric substrate," *IEEE Trans. Microwave Theory Tech.*, vol. MTT-23, pp. 541–548, July 1975.

[5] T. Kitazawa, Y. Hayashi, and M. Suzuki, "A coplanar waveguide with thick metal-coating," *IEEE Trans. Microwave Theory Tech.*, vol. MTT-24, pp. 604–608, Sept. 1976.

[6] G. Ghione and C. U. Naldi, "Coplanar waveguide for MMIC applications: Effect of upper shielding conductor backing, finite-extent ground planes, and line-line coupling," *IEEE Trans. Microwave Theory Tech.*, vol. MTT-35, pp. 260–267, Mar. 1987.

[7] G. C. Liang, Y. W. Liu, and K. K. Mei, "Full-wave analysis of coplanar waveguide and slotline using the time-domain finite-difference method," *IEEE Trans. Microwave Theory Tech.*, vol. 37, pp. 1949–1957, Dec. 1989.

[8] B. E. Kretch and R. E. Collin, "Microstrip dispersion including anisotropic substrates," *IEEE Trans. Microwave Theory Tech.*, vol. MTT-35, pp. 710–718, Aug. 1987.

[9] C. J. Hsu and R. E. Collin, "Microstrip open-end and gap discontinuities including anisotropic substrates," *Electromag.*, vol. 15, pp. 527–545, 1995.

[10] C. J. Hsu, "Microstrip discontinuities and coplanar waveguide dispersions and discontinuities including anisotropic substrates," Ph.D. dissertation, Dept. Elect. Eng., Case Western Reserve University, Cleveland, OH, 1994.

Chung Jen Hsu (S'91–M'93) received the B.S. and M.S. degrees in communication engineering from the National Chiao Tung University, Hsinchu, Taiwan, R.O.C., in 1984 and 1986, respectively, and the Ph.D. degree in electrical engineering and applied physics from Case Western Reverse University, Cleveland, OH, in 1994.

From 1984 to 1986, he was an Electronics Engineer at Microelectronic Technology Inc., Hsinchu, Taiwan, R.O.C., where he developed 18- and 23-GHz MESFET phase detectors in phase-locked loop (PLL) for short-haul digital microwave communications. During his compulsory two-year military service from 1986 to 1988, he was a Second Lieutenant Lecturer at the Army Communication and Electronics Senior High School, Taiwan, R.O.C. After his discharge from the Army, he joined ERSO/ITRI, Chutung, Taiwan, R.O.C., as an Associate Engineer (until 1989), where he developed GaAs monolithic-microwave integrated-circuit (MMIC) power amplifiers for mobile phones. During the 1991–1992 academic years, he was a Teaching Assistant at Case Western Reverse University. From 1994 to 1995, he was a Project Manager, during which time he developed GaAs MMIC subsystems, with Hexawave Inc., Hsinchu, Taiwan, R.O.C. In 1996, he joined Samsung Microwave Semiconductor, as a Senior MMIC Design Engineer (until 1998), during which time he designed personal communication system (PCS) and 2.4-GHz ISM band GaAs MMIC power amplifiers. From 1998 to 2000, he was with Diablo/Cadence, as a Senior radio-frequency integrated circuit (RFIC) Design Engineer, during which time he designed broad-band buffers for probing applications, ultrahigh-speed mixed-signal application-specific integrated circuits (ASICs) for missile's three-dimensional (3-D) imaging laser radar detection for National defense, and 900-MHz RFIC transceivers, spread-spectrum baseband processors and baluns for wireless utility meter reading. In 2000, he was with eWave System Inc., Santa Clara, CA, as an RFIC Design Manager, where he developed RFICs for wireless communication and internet applications. His current research interests include the numerical analysis of microwave planar integrated circuits, the modeling of microwave active devices, and the design of microwave integrated circuits (MICs), MMICs, and RFICs.